

Dielectric and Thermodynamic Study on the Liquid Crystal Dimer α -(4-Cyanobiphenyl-4'-oxy)- ω -(1-pyreniminebenzylidene-4'-oxy)undecane (CBO11O·Py)

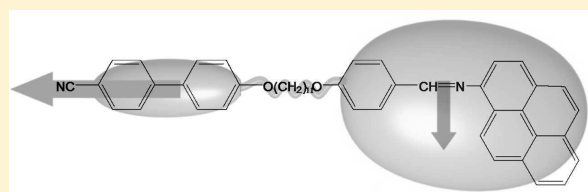
N. Sebastián,[†] M. R. de la Fuente,[†] D. O. López,^{†,‡,*} M. A. Pérez-Jubindo,[†] J. Salud,[‡] S. Diez-Berart,[‡] and M. B. Ros[§]

[†]Departamento de Física Aplicada II, Facultad de Ciencia y Tecnología, Universidad del País Vasco, Apartado 644, E-48080 Bilbao, Spain

[‡]Grup de Propietas Físiques dels Materials (GRPFM), Departament de Física i Enginyeria Nuclear, E.T.S.E.I.B. Universitat Politècnica de Catalunya, Diagonal, 647 08028 Barcelona, Spain

[§]Departamento de Química Orgánica, Facultad de Ciencias, Instituto de Ciencia de Materiales de Aragón, Universidad de Zaragoza-CSIC, 50009 Zaragoza, Spain

ABSTRACT: Broadband dielectric spectroscopy (10^3 to 1.8×10^9 Hz) and specific heat measurements have been performed on the odd nonsymmetric liquid crystal dimer α -(4-cyanobiphenyl-4'-oxy)- ω -(1-pyreniminebenzylidene-4'-oxy)undecane (CBO11O·Py), as a function of temperature. The mesogenic behavior is restricted to a nematic mesophase which can be supercooled down to its corresponding glassy state if the cooling rate is fast enough (no less than $15\text{ K}\cdot\text{min}^{-1}$). Dielectric measurements enable us to obtain the static permittivity and information about the molecular dynamics in the nematic mesophase as well as in the isotropic phase and across the isotropic-to-nematic phase transition. Two orientations (parallel and perpendicular) of the molecular director with regard to the probe electric field have been investigated. In the nematic mesophase, the dielectric anisotropy is revealed to be positive. Measurements of the parallel component of the dielectric permittivity are well explained by means of the molecular theory of dielectric relaxation in nematic dimers (J. Chem. Phys. 2004, 121 (16), 8079). The dimer is seen as a mixture of cis and trans conformers, and the model allows us to estimate their relative populations at each temperature. The main molecular motions are interpreted by the model as independent end-overend rotations of each terminal semirigid unit of the dimer. The nematic-to-isotropic phase transition has been exhaustively studied from the accurate evolution of the specific-heat and the static dielectric permittivity data. It has been concluded that the transition is first order in nature and follows the tricritical hypothesis. As a consequence, the nematic mesophase has been characterized as uniaxial despite the biaxiality and flexibility of the dimer molecule.



1. INTRODUCTION

Liquid crystals are a kind of molecular materials in which the constituent molecules obligatory possess shape anisotropy. Stability of liquid crystal phases or mesophases is determined by the molecular shape of the constituents and so the mesophase behavior has long been recognized as molecular shape-dependent. It is well-known how rod-shaped molecules, disk-shaped molecules, and bent-shaped molecules induce their own hierarchy of mesophases of different symmetries. Of course, there are some specific mesophases, the nematic for instance, which can form from different molecular shapes.

Molecular flexibility is one of the most important structural aspects which may influence the molecular shape. In most of the liquid crystals, terminal flexible alkyl chains are attached to anisotropic molecular cores. However, there is a group of liquid crystal-forming molecules in which semirigid terminal groups are linked via flexible spacers. Such compounds are known as liquid crystal oligomers^{1–3} and the simplest of these compounds are the so-called liquid crystal dimers which consist of two terminal groups connected by a flexible spacer. These compounds have

attracted considerable attention during the last years.^{3–17} At the beginning, the semirigid units were usually calamitic-core moieties although discotic-core moieties have also been proposed.³ Currently, combinations of bent-core with calamitic-core moieties or even only bent-core moieties are being explored.^{4–9}

Liquid crystal dimers are commonly classified in two broad classes: symmetric and nonsymmetric. In a symmetric liquid crystal dimer the two semirigid units are identical, whereas they are different in a nonsymmetric dimer. In both classes, the phase behavior is quite different to that observed for conventional calamitic low molar mass liquid crystals. Three particular aspects of the constituent molecules must be considered: the nature of the flexible linking chain (the vast majority are alkyl chains but other less usual are siloxane chains), the chain length (as determined by the number of linking groups) and the parity of the chain (even or odd numbers of linking groups). For a given

Received: March 25, 2011

Revised: July 4, 2011

Published: July 12, 2011

species of chain, the chain length plays an important role on mesophase properties. Short chains give rise to nearly rigid molecules because the two terminal groups are strongly coupled orientationally. Conversely, for long chains both terminal groups are quite independent and some properties of the mesophases are similar to those of the monomers that form the dimer moieties. The parity of the chain strongly influences some mesophase properties exhibiting pronounced odd–even effects in transition temperatures and transitional entropies. Even members of a given dimeric series exhibit higher values than odd compounds and this fact, well explained in some theoretical approaches,^{18–22} has been attributed to the dependence of the energetically favored molecular shapes (*conformers*) on the parity of the flexible chain. It should be stressed that the distribution of conformers between the accessible states is temperature-dependent over the range of the mesophase.

Liquid crystal dimers with polar terminal groups are of great interest because one of the properties that is particularly sensitive to changes in molecular shape is the dielectric permittivity. Dielectric measurements have provided information on the temperature dependence of the distribution of conformers in liquid crystal phases and have allowed to gain insight into the rotational dynamics of the dipolar groups of the dimer. So far, few studies devoted to the dielectric properties of liquid crystal dimers have been published.^{5,6,10,17,23–27} Some of these reported data on symmetric and nonsymmetric dimers have prompted the development of new theoretical models to explain the results. Of particular interest in the context of this paper is the formulation of the theory¹¹ for the dielectric relaxation of mesogenic dimers in a nematic phase based on a time-scale separation for the motion of the flexible chain and the terminal end groups. The details of such a model will be given later. It results evident that in order to promote more complex and refined theories, dielectric experimental results on a great variety of structurally different liquid crystal dimers have to be obtained. This provides one of the motivations for the work described in this paper.

Another motivation is the current interest in bent molecules with clear biaxial shapes as potential candidates of thermotropic liquid crystals presenting the elusive biaxial nematic phase (N_B).^{28,29} However, it has been recently claimed that in addition to the biaxial shape of molecules, a certain flexibility seems to be required to stabilize the N_B phase by coupling the orientational order with the conformational distribution.³⁰ In the past, it has been theorized that the isotropic (I)-to- N_B phase transition must be second order and takes place at the Landau point.^{31,32} This fact is in contrast with the I-to-uniaxial nematic (N_U) phase transition which has been theorized as (weakly) first order in nature.^{33,34} It is clear that accurate experimental studies on the nature of the N-to-I phase transition in liquid crystal dimers which are currently absent may give insights into the nature of the nematic mesophase as well as the mechanisms involved in the phase transition.

The liquid crystal dimer α -(4-cyanobiphenyl-4'-yloxy)- ω -(1-pyrenimine-benzylidene-4'-oxy) undecane which can be referred, in what follows, by the acronym CBO11O·Py, is a semiflexible compound that exhibits liquid crystal phase behavior. According to the previous work of Attard and co-workers,³⁵ the reported mesophase sequence on cooling from the isotropic phase (I) includes only a nematic mesophase (N) that may be vitrified if cooled fast enough.

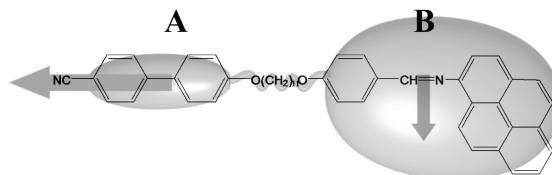
Thus, the molecule of CBO11O·Py consists of two different terminal groups being an archetypal nonsymmetric liquid crystal

dimer with a rather simple mesogenic behavior which has not been the subject of dielectric experimental studies yet. These results are of particular importance for comparison purposes with Stocchero's model calculations.¹¹ On the other hand, both the N mesophase and the phase transition N-to-I have been previously examined in a rather qualitative way.³⁵ Results from higher-resolution experiments are clearly desirable.

The structure of the paper is as follows. In section 2, we describe the experimental details. In section 3, we present and discuss results concerning: the overall thermal behavior on the basis of specific heat data and microscopic observations, dielectric measurements on both the isotropic and nematic phases and finally very accurate specific heat as well as static dielectric data through the nematic (N)-to-isotropic(I) phase transition. The concluding remarks are summarized in section 4.

2. EXPERIMENTAL METHODS

2.1. Material. The schematic molecular structure of CBO11O·Py is



It consists of two terminal groups with different shape and size (named A and B in the scheme) attached by a flexible spacer of 11 methylene units. The terminal group A has an important dipole moment along its long axis associated with the nitrile group, while the B group has a smaller and mainly transverse dipole moment (drawn in the scheme as perpendicular) associated with the imine group. The transverse dipole moment of the ether linkages will be neglected due to its much smaller value. The material has been synthesized according to a previous work of Attard et al.³⁵

2.2. Experimental Techniques. Specific heat data at normal pressure were obtained by means of a commercial differential scanning calorimeter DSC-Q2000 from TA-Instruments working in modulated mode (MDSC). It is important to realize that similarly to an AC-calorimeter, MDSC-technique, besides specific-heat data, simultaneously provides phase shift angle data (ϕ , the phase lag between the modulated temperature rate and the modulated heat flow). In our work, the experimental conditions (temperature amplitude and oscillation period) were adjusted to only get the real part (the static part) of the complex specific-heat in such a way that the phase lag angle is nearly zero and consequently, the imaginary part of the complex specific-heat data vanishes. However, when a first order phase transition takes place at a certain temperature, there exists a region around this temperature (the coexistence region) where the ϕ -angle cannot be kept as zero. Likewise, by means of a special calibration procedure in which very precise latent heat data measured from other homologous-compounds through adiabatic calorimetry are considered, MDSC-technique is also suitable for quantitative measurements of latent heats of first order transitions, even if they are weak. A more detailed description of the MDSC technique can be found somewhere else.^{36,37}

The MDSC measurements were made following two different procedures. The first one, thought as a standard study of the overall thermal behavior of the sample, consisted of heating runs at $1 \text{ K} \cdot \text{min}^{-1}$ from room temperature up to the I-phase and cooling runs at several cooling rates to observe glassy behavior if possible. The second procedure, designed to study the nature of the N-to-I phase transition, consisted of heating and cooling runs in a temperature interval of 5 K around the transition at $0.01 \text{ K} \cdot \text{min}^{-1}$. For both procedures, the parameters of modulation (temperature amplitude and oscillation period) were $\pm 0.5 \text{ K}$ and 60 s in the standard and $\pm 0.07 \text{ K}$ and 23 s in the other. The sample masses (chosen between 2 and 3 mg) were selected to ensure a uniform thin layer within the aluminum pans.

Measurements of the complex dielectric permittivity $\epsilon^*(f) = \epsilon'(f) - i\epsilon''(f)$, in the range 10^3 to $1.8 \times 10^9 \text{ Hz}$, were performed using two impedance analysers: the HP 4192A and 4291A. The cell consists of two gold-plated brass electrodes (diameter 5 mm) separated by thick silica spacers of the order of $50 \mu\text{m}$. A modified HP16091A coaxial test fixture was used as the sample holder. It was held in a cryostat from Novocontrol and both temperature and dielectric measurements were computer-controlled. Additional details of the experimental technique can be found elsewhere.^{37,38}

Dielectric measurements were performed on heating and on cooling with different temperature steps being stabilized to $\pm 20 \text{ mK}$.

Optical textures were studied with an Olympus polarizing microscope equipped with a Linkam THMSG-600 hot stage and a Linkam TMS-94 temperature controller.

3. RESULTS AND DISCUSSION

3.1. Thermal Behavior. Schlieren textures characteristic of the nematic mesophase were observed in thin films near the N-to-I phase transition (see Figure 1). As can be observed from this figure, 2-fold brushes are mostly found though some 4-fold brushes may also be observed.

On cooling the sample from the nematic phase at ordinary cooling rates ($1\text{-}5 \text{ K} \cdot \text{min}^{-1}$) crystallization occurs at about 380 K. However, at cooling rates of $15 \text{ K} \cdot \text{min}^{-1}$ or higher, the nematic mesophase vitrifies. Figure 2 shows the specific heat as a function of temperature for a sample that has been cooled from the I-phase (gray symbols) down to about 390 at $1 \text{ K} \cdot \text{min}^{-1}$. The I-to-N phase transition can be clearly observed in the inset of Figure 2, in both heating and cooling runs. Figure 2 also shows the specific heat as a function of temperature for the sample on a heating run at $1 \text{ K} \cdot \text{min}^{-1}$ from its nematic glassy state (denoted as N_{gl} in Figure 2). On heating, once the glass transition occurs at T_{gl} (see Table 1 our reported value along with that reported by Attard et al.), the nematic mesophase becomes metastable, denoted as supercooled nematic phase (N_{spc}). At about 320 K, an irreversible transition to the solid crystalline phase (Cr) takes place. The heating up to about 440 K shows both the Cr-to-N and the N-to-I phase transitions at about 5 K apart. However, as cited above, on cooling, the N-mesophase can be supercooled down to about 45 K below the N-to-I phase transition, remaining as a metastable phase but without apparent tendency to crystallize. A subsequent heating enables us to obtain only the N-to-I phase transition. The temperatures associated with both the Cr-to-N and the N-to-I phase transitions, along with those values coming from the literature, are gathered in Table 1.

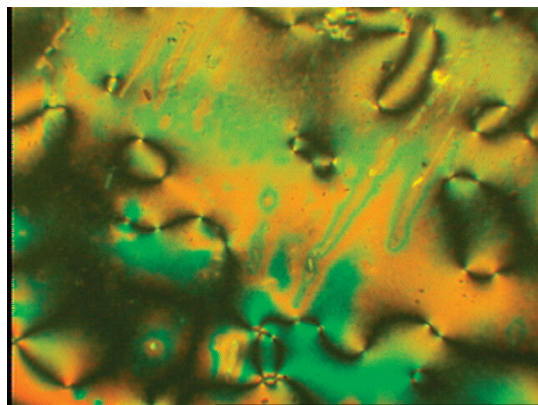


Figure 1. Classical Schlieren texture of the CBO11O·Py at 420 K.

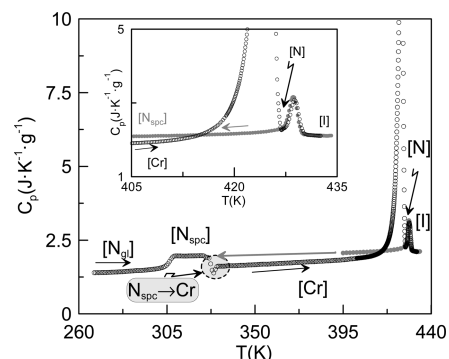


Figure 2. - Specific-heat data as a function of temperature of a sample of CBO11O·Py which has been previously cooled from the I-phase at $15 \text{ K} \cdot \text{min}^{-1}$ (black and gray symbols are collected on heating and cooling runs at $1 \text{ K} \cdot \text{min}^{-1}$, respectively). The inset shows in a zoom window the specific heat around both the Cr-to-N and the N-to-I phase transitions on heating (black symbols) and on cooling (gray symbols) at $1 \text{ K} \cdot \text{min}^{-1}$.

The total enthalpy change associated with any transition (ΔH^{TOT}) can be written as:

$$\Delta H^{\text{TOT}} = \Delta H + \int \Delta C_p \, dT \quad (1)$$

where the second term of the right-hand of eq 1 is the pretransitional fluctuation contribution (ΔC_p being the difference $C_p - C_{p,\text{background}}$ due to the change of orientational order intrinsic to this transition) and the latent heat is ΔH which vanishes for second order transitions. In strongly first order phase transitions, the second term of the righ-hand of eq 1 can be neglected in front of the latent heat and the total enthalpy change is identified with the latent heat associated with the phase transition. This is the case of the Cr-to-N phase transition of CBO11O·Py. However, in weakly or very weakly first order phase transitions the second term of the righ-hand of eq 1 could be comparable with the latent heat and thus, the total enthalpy cannot be considered as the latent heat. The case of the N-to-I phase transition of CBO11O·Py may be an example of this and will be considered later in detail.

The resulting latent heat for the Cr-to-N phase transition obtained by using eq 1 in which the second term of the right-hand

Table 1. Transition Temperatures (T_{CrN} and T_{NI}) and associated latent heats (ΔH_{CrN} and ΔH_{NI})

T_{CrN} (K)	ΔH_{CrN} (kJ·mol ⁻¹)	T_g (K)	T_{NI} (K)	ΔH_{NI} (kJ·mol ⁻¹)	ref
423.2 ^{a,b}	64.03 ^b	307.2 ^{a,b}	432.2 ^{a,b}	1.80 ^b	35
421.3 ± 0.5	63.4 ± 0.2	305.0	426.9 ± 0.5	0.5 ± 0.1	this work

^a Temperatures were obtained from the peak maximum in the DSC-traces at 10 K·min⁻¹. ^b Measurements are performed with a Perkin-Elmer DSC-7.

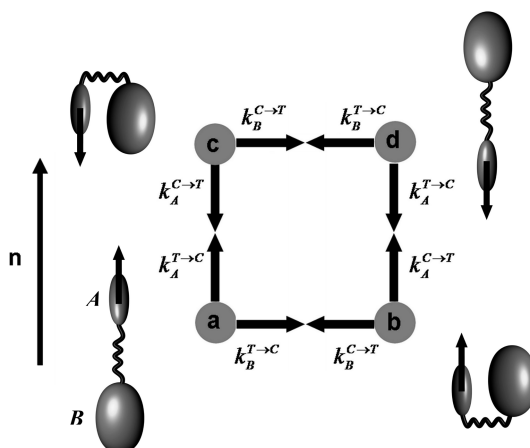


Figure 3. Schematic representation of the four stable states for nonsymmetric dimers, according to Stocchero et al.'s¹¹ theoretical model.

can be neglected is reported in Table 1 together with the value read from the literature.

3.2. Dielectric Behavior. *3.2.1. Theoretical Background.* The different theories of Maier–Meier³⁹ for the static permittivity and Nordio–Rigatti–Segre⁴⁰ for the molecular dynamics assume that the constituent molecules are rigid. Although these models have been revealed to be very useful to interpret the dielectric data on liquid crystal monomers,^{27,38,41,42} for liquid crystal dimers the model of Stocchero et al.¹¹ which is a four-state model, has proven great success in interpreting the experimental results.

Previously published data¹⁰ on the dielectric properties of the nematic mesophase of symmetric and nonsymmetric dimers showed some unexpected results. In the case of symmetric dimers, the parallel and perpendicular components of the static dielectric permittivity were found to decrease rapidly with decreasing temperature suggesting a change in the distribution of chain conformations with temperature. On the contrary, for nonsymmetric dimers, for which there is a net longitudinal component of the molecular dipole moment for all conformers, the variation of the static permittivity components was found to be similar to that observed for monomeric mesogens with positive dielectric anisotropy. In addition, two low frequency relaxation processes, whose strengths seemed to be correlated in temperature, were observed. Such results suggested that it is possible to get information on the changes of conformational distribution in the nematic phase from measurements of the dielectric permittivity as a function of frequency and temperature. This prompted Stocchero et al.¹¹ to formulate a theoretical model for nematogenic liquid crystal dimers that takes into account the orientational effect of the nematic phase by a generalization of the Maier–Saupe potential⁴³ and models the flexibility of the spacer by a full torsional potential for the carbon–carbon bonds of the chain. Calculations showed that in the mixing of trans (extended configuration) and cis (bent

configuration) conformers, trans-conformers population increases with order and in addition, becomes more extended. As a result, for symmetric dimers the mean square dipole moment decreases with order and the value of the static permittivity as well. Moreover, for a nonsymmetric dimer where only one of the semirigid units exhibits a dipole moment, the change of the conformation of the molecule has no impact on the mean square dipole moment, and then the static permittivity is predicted to behave as in liquid crystal monomers with positive dielectric anisotropy.

The original model of Maier–Saupe⁴³ for the dielectric relaxation of a dipolar molecule in a nematic potential was a two-state model representing the two orientations of a dipole along the director axis. In the case of the model of Stocchero et al., for high enough order parameters the resulting potential presents four deep wells that correspond to the four stable states of the dimer in which the terminal groups A and B align parallel or antiparallel to the director, as shown in Figure 3 where the model is summarized. Assuming that the chain dynamics is fast enough not to influence the relaxation of the dipolar terminal groups, the potential provides the basis of the kinetic model of dielectric relaxation in nematic dimers which considers that only the independent end-overend rotations of each unit are allowed. The simultaneous rotations of the two rigid units (i.e., $a \leftrightarrow d$ and $b \leftrightarrow c$ in Figure 3) are excluded because they are associated with the passage through a potential maximum. The relative rates for flipping of the different rigid units are determined by their rotational diffusion coefficients, and the nematic potential experienced by the terminal groups. It should be stressed that for high enough order parameters a time-scale separation is achieved between the slow end-overend rotations and the fast processes that appear at higher frequencies, i.e. the rotation around the long axis and the precession around the director, that are not dealt in the model. Consequently, these high frequency modes will be tentatively described in the same terms as in liquid crystal monomers.⁴⁴

Calculations based on the model¹¹ for symmetric dimers predict a single relaxation time for the parallel component of the dielectric permittivity with an intensity that diminishes with decreasing temperature (or increasing order) in a quite good agreement with experimental determinations.^{10,11,17,27} The results for nonsymmetric dimers depend on the shape and dipole moments of the different rigid units. The different cases have been extensively analyzed somewhere else.¹¹ Experimental results¹⁰ even being very scarce are in agreement with predictions.

By applying the model¹¹ to the nonsymmetric dimer CBO11O·Py, only the longitudinal component of the permittivity has been considered. Consequently, for the low frequency spectra, only the dipole moment of the A terminal unit has been taken into account. It should be stressed that the smaller and mainly transverse dipole moment of the B terminal unit only contributes to the high frequency modes. For this case (dimers with two different terminal units with only one longitudinal dipole moment located in the smaller one) a two exponential

correlation function is considered:

$$C_{\parallel\parallel}(t) = \langle u_{\parallel}^2 \rangle (P_T^{eq} - P_C^{eq})^2 \exp(-2k_B t) + 4\langle u_{\parallel}^2 \rangle (P_T^{eq} P_C^{eq})^2 \exp(-2k_A t) \quad (2)$$

where P_T^{eq} and P_C^{eq} are the relative equilibrium populations of the trans and cis conformers of the dimer at each temperature and k_A and k_B are the effective rates of the flipping motions.¹¹ This correlation function is associated with two relaxation processes in the dielectric spectra, see Figure 3. The first of them at low frequencies which is consequence of the flip-flop motion of the B unit (denoted hereafter as $m_{1,L}$ -mode), that although does not have longitudinal dipole moment drives a further and immediate transition of the A unit. The other relaxation at higher frequencies involves a flip-flop of the smaller group (denoted hereafter as $m_{1,H}$ -mode). The amplitudes of both modes, $m_{1,L}$ and $m_{1,H}$, depend on $(P_T^{eq} - P_C^{eq})^2$ and $P_C^{eq} P_T^{eq}$, respectively. The interchange cis-to-trans as temperature decreases involves the concerted change of the amplitude of the modes; that of the $m_{1,H}$ decreases while the other increases.

3.2.2. Dielectric Measurements and Analysis. Measurements of the static dielectric permittivities (limiting low frequency permittivity) of the nonsymmetric dimer CBO11O·Py are shown in Figure 4 as a function of temperature. In metal cells, planar alignment was obtained without any treatment, allowing to measure the static perpendicular permittivity (ε_{\perp}). The material has a positive dielectric anisotropy ($\Delta\varepsilon = \varepsilon_{\parallel} - \varepsilon_{\perp}$), and so the parallel component of the permittivity (ε_{\parallel}) was obtained by applying a bias electric field (25 V). Figure 4 shows that both components of the static permittivity (ε_{\perp} and ε_{\parallel}) and the mean permittivity ($\varepsilon_{Mean} = 1/3[\varepsilon_{\parallel} + 2\varepsilon_{\perp}]$) change with temperature as in typical liquid crystal monomers with positive dielectric anisotropy, as predicted by the theoretical model of Stocchero et al.¹¹ It can also be observed how the mean permittivity experiments a small positive increment at the N-to-I phase transition.

The temperature and frequency dependence of the imaginary part of the permittivity is shown in the three-dimensional plot of Figure 5 for parallel and perpendicular alignments. At first glance, in the parallel alignment, two main relaxation modes that seem to be correlated as the theoretical model predicts¹¹ are observed.

Let us consider the real and imaginary parts of the permittivity in the parallel and perpendicular alignments as a function of frequency for both the nematic mesophase and the isotropic phase at two characteristic temperatures (Figure 6) for the purpose of illustrating the data analysis. As it can be observed in the dielectric loss peaks of Figure 6, different relaxation modes appear partially superimposed. The frequency dependence of the permittivity has been analyzed using the empirical function

$$\varepsilon(\omega) = \sum_k \frac{\Delta\varepsilon_k}{[1 + (i\omega\tau_k)^{\alpha_k}]^{\beta_k}} + \varepsilon_{\infty} - i \frac{\sigma_{dc}}{\varepsilon_0} \quad (3)$$

where $\Delta\varepsilon_k$ is the dielectric strength of each relaxation mode, τ_k the relaxation time related to the frequency of maximum dielectric loss, α_k and β_k are parameters which describe the shape (symmetry and width) of the relaxation spectra ($\alpha_k = \beta_k = 1$ corresponds to Debye relaxation) and σ_{dc} is the dc conductivity. The summation is extended over all relaxation modes, and each one is fitted according to the Havriliak–Negami (H–N) function.

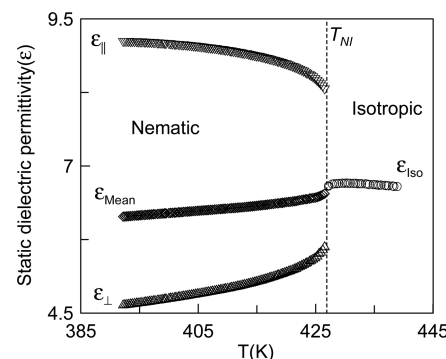


Figure 4. Static dielectric permittivity behavior in the I and N phases of CBO11O·Py. Open up and down triangles stand for ε_{\parallel} and ε_{\perp} , respectively; open diamonds and circles stand for ε_{Mean} and ε_{Isot} , respectively.

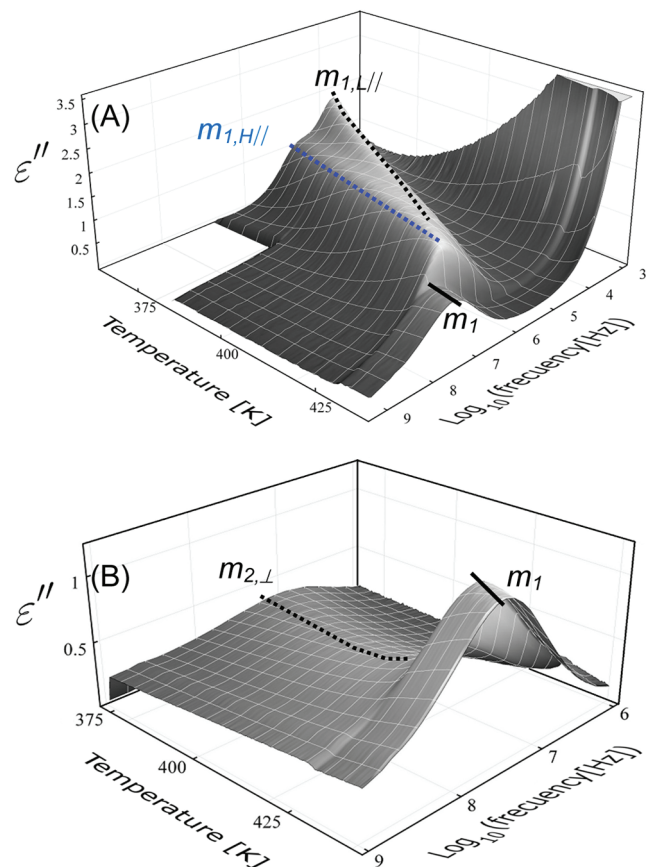


Figure 5. Three-dimensional plot of dielectric losses vs temperature and logarithm of the frequency for CBO11O·Py in parallel (A) and perpendicular (B) alignments.

Figure 6A shows, as an example, the real and imaginary parts of the dielectric permittivity measured as a function of frequency in the I-phase at 433 K. The results were fitted, according to eq 3, to only one mode ($\alpha = 0.87$; $\beta = 0.63$). Because of the lack of order, this contribution could be attributed to a concerted rotation of the whole dimer denoted as the m_1 -mode.

Figure 6B shows typical dielectric relaxation curves for the real and imaginary parts as a function of frequency in the N-mesophase (parallel alignment with bias electric field) at

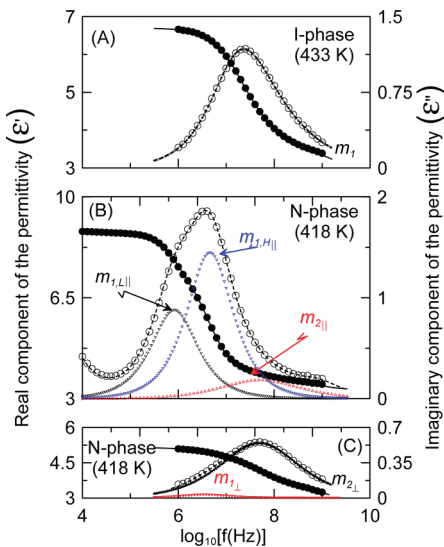


Figure 6. Frequency dependence of the dielectric permittivity of CBO11O·Py in the isotropic phase ($T = 433\text{ K}$) (A) and in the nematic phase ($T = 418\text{ K}$) in both the parallel (B) and perpendicular (C) alignments. Black solid and dashed lines are fittings according to eq 3. Symbol-lines represent deconvolution into elementary modes. For simplicity, the direct current conductivity contribution (σ_{dc}) is not drawn, but is considered in the fitting procedure.

418 K. The results were fitted, according to eq 3, to three relaxation processes. The low frequency relaxation (Debye-like) is identified with the $m_{1,L}$ -mode predicted by the model¹¹ and thus, is considered to be due to changes in the orientation of the B terminal group via changes in the conformational state of the flexible spacer of the dimer denoted hereafter as the $m_{1,L||}$ -mode. The intermediate frequency relaxation (Debye-like) is identified with the $m_{1,H}$ -mode according to the theoretical model.¹¹ This relaxation is attributed to changes in the orientation of the A group via changes in the conformational state of the flexible spacer of the dimer and denoted hereafter as the $m_{1,H||}$ -mode. Figure 5A qualitatively shows how the amplitude of both relaxations is correlated over the temperature range. Additionally, there is another relaxation ($\alpha = 0.69$; $\beta = 1$) at higher frequencies that could be mainly attributed to the rotation around the molecular long axis, and then, related to the transverse dipole moment, as described by the Nordio–Rigatti–Segre theory.⁴⁰ It will be denoted hereafter as the $m_{2||}$ -mode.

Figure 6C shows, as an example, both components (real and imaginary parts) of the dielectric permittivity in the N mesophase (with the sample in perpendicular alignment) at 418 K. Two relaxation modes can be observed and fittings have been performed through eq 3. The low frequency mode has been associated with the end-overend rotation of the terminal units. Because of its small dielectric strength, the authors attribute this mode to a nonperfect perpendicular alignment of the director (for coherence we denote this mode as $m_{1\perp}$) and will be ignored in subsequent analysis. The high frequency mode, the most prominent in the perpendicular alignment ($\alpha = 0.69$; $\beta = 1$), could be attributed to the superposition of the precessional motions of the semirigid units and the rotation of the molecule around its long axis. This mode will be denoted as the $m_{2\perp}$ -mode.

Figure 7A shows the temperature dependence of the dielectric strength data for all the aforementioned relaxation modes in both alignments. In parallel alignment, when comparing the dielectric

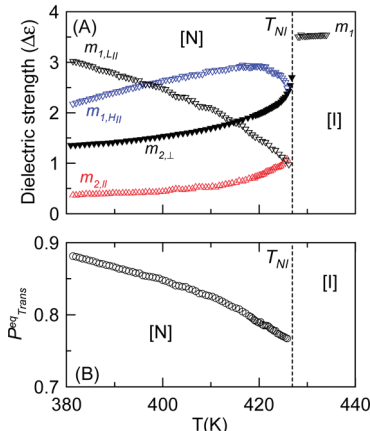


Figure 7. (A) Dielectric strength data as a function of temperature of the different elementary contributions for CBO11O·Py. (B) Calculated equilibrium population of trans-conformers vs temperature in the nematic phase of CBO11O·Py.

strengths of the $m_{1,L||}$ -mode ($\Delta\epsilon_{m1,L||}$) and $m_{1,H||}$ -mode ($\Delta\epsilon_{m1,H||}$) it clearly appears that they are linked as the temperature changes. A decrease in temperature causes $\Delta\epsilon_{m1,H||}$ to decrease, while $\Delta\epsilon_{m1,L||}$ increases. The dielectric strength of the $m_{2||}$ -mode ($\Delta\epsilon_{m2||}$) decreases on entering the N-mesophase stabilizing in a nearly constant value at lower temperatures as previously reported for other dimers in which the same mode has been identified.^{10,17,27} In perpendicular alignment, the most prominent contribution comes from the high frequency relaxation ($m_{2\perp}$ -mode). Its dielectric strength ($\Delta\epsilon_{m2\perp}$) evolves with temperature, in a certain extent, similar to $\Delta\epsilon_{m2||}$, as is expected.

The dielectric data of the nonsymmetric dimer CBO11O·Py allows us to provide a more quantitative description of the changes of the conformational distribution in the nematic phase. According to the model, in the N-mesophase, the ratio of dielectric strengths of both $m_{1,L||}$ - and $m_{1,H||}$ -modes can be easily expressed as a function of the equilibrium population of trans conformers

$$\frac{\Delta\epsilon_{m1,L||}}{\Delta\epsilon_{m1,H||}} = \frac{(2P_T^{eq} - 1)^2}{4P_T^{eq}(1 - P_T^{eq})} \quad (4)$$

From eq 4 P_T^{eq} as a function of temperature is obtained. Figure 7B shows how P_T^{eq} increases as temperature decreases, corresponding to an increase in the orientational order. Within the assumptions of the model, the proportion of trans conformers changes from 77% (23% of cis conformers) to 88% (12% of cis conformers) over the temperature of the studied nematic range. In fact, it is important to realize that the model predicts the absence of the $m_{1,L||}$ -mode when the proportion of both trans and cis conformers is the same.

Figure 8 shows, in an Arrhenius plot, the temperature dependence of the characteristic relaxation frequencies associated with each mode for both the N and I phases. Activation energies for the $m_{1,L||}$ ($E_a^{m1,L||}$) and $m_{1,H||}$ ($E_a^{m1,H||}$) relaxation modes are about 110 and 90 kJ·mol⁻¹, respectively. The ratio ($E_a^{m1,H||}/E_a^{m1,L||}$) is about 0.8 which is of the same order that what has been found for the nonsymmetric dimer α -(4-cyanobiphenyl-4'-yloxy)- ω -(4-decylaniline-benzylidene-4'-oxy) nonane (denoted as CBO9O·10).^{10,11} Thus, the energy barriers for the motions of the larger terminal groups in relation to the smaller polar ones are

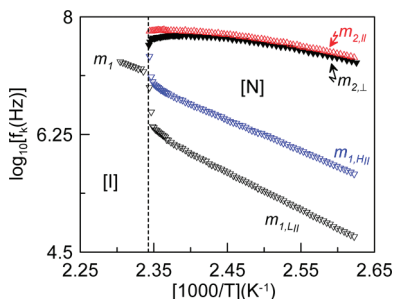


Figure 8. Arrhenius plot of the relaxation frequencies (f_k) of the different elementary contributions for CBO11O·Py.

in the same proportion despite the chain length, shorter for the CBO9O·10 than for the CBO11O·Py. This fact could be explained as due to combined effect of the larger size and less anisotropic shape of the larger terminal group of CBO11O·Py. As for the so-called $m_{2,||}$ or $m_{2,\perp}$ relaxation modes, the corresponding activation energies ($E_a^{m_{2,||}}$ or $E_a^{m_{2,\perp}}$) are of about $40 \text{ kJ} \cdot \text{mol}^{-1}$, a value twice of what has been found for the same modes in CBO9O·10.^{10,11}

3.3. The Nematic-to-Isotropic Phase Transition. *3.3.1. Theoretical Background.* On the theoretical level, one of the simplest description of the N_U (or N_B)-to-I phase transition is that offered by a sixth-order Landau–de Gennes free energy expansion of the nematic phase in terms of traces of powers of the second rank symmetric traceless order parameter tensor Q :³⁴

$$\begin{aligned} F_N = F_I + \frac{1}{2} A Tr Q^2 - \frac{1}{3} B Tr Q^3 + \frac{1}{4} C [Tr Q^2]^2 \\ + \frac{1}{5} D [Tr Q^2][Tr Q^3] + \frac{1}{6} E [Tr Q^2]^3 + \dots \end{aligned} \quad (5)$$

where A, B, C, D, E are coefficients of the expansion and F_I is the free energy of the isotropic phase. In general, A is defined as $a_0(T - T^*)$ with $a_0 > 0$ and T^* is the spinodal temperature accounting for the metastable limit of the I phase; the other terms B, C, D, E are assumed to be temperature independent and the term B may be considered, as an approximation, proportional to powers of $(T^{**} - T^*)$ where T^{**} is the spinodal temperature accounting for the metastable limit of the N mesophase.

Regardless of the definition of Q , the existence of the term B no null in eq 5, the so-called cubic invariant is the responsible of the first order character of the N-to-I phase transition. The uniaxiality of the nematic phase seems to be connected with the existence of the cubic invariant, or in other words, for a biaxial nematics, the cubic invariant B is null. Several factors, among them, the biaxiality and flexibility of the molecules forming a uniaxial nematic phase diminishes the absolute value of B ,³⁴ but it does not vanish. As a limit case, suggested earlier by Keyes⁴⁵ and Anisimov,³⁴ is the N-to-I tricritical phase transition for which B is very small and A and C parameters become simultaneously zero with a specific-heat critical exponent α on both the N and I phases of $1/2$ and an order parameter critical exponent β of $1/4$.

From a experimental point of view, accurate specific heat and static dielectric data through the N-to-I phase transition may provide both spinodal temperatures T^{**} and T^* as well as both α and β critical exponents.

Let us consider the above considerations to be applied to biaxial and flexible molecules of CBO11O·Py.

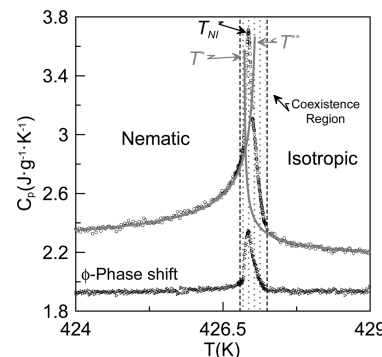


Figure 9. Specific heat data (open circles) as a function of temperature near the N-to-I phase transition of the CBO11O·Py. Phase shift angle (ϕ) data (open triangles) are included to delimit the specific heat coexistence region (shaded area). Gray solid lines are fittings according to eqs 6a and 6b.

3.3.2. Specific-Heat Measurements Analysis. Figure 9 shows the specific heat and the δ -phase shift data in a region of about $\pm 2 \text{ K}$ around the N-to-I phase transition. The sharp-peak in δ -phase shift data at the transition temperature is a signature of the first order character of the N-to-I phase transition. The peak in δ will be used to delimit the coexistence region, shown as a shaded area in Figure 9. The standard expressions^{34,38,46} used to proceed with such an analysis in the N and I phases, considered to be valid in a region of no more than $\pm 3 \text{ K}$ around T_{NI} but excluding all the points in the coexistence regions are:

$$C_{p,I} = B_C + D_C \left[\frac{T}{T^*} - 1 \right] + A_{C,I} \left| \frac{T}{T^*} - 1 \right|^{-\alpha} \quad \text{for } T > T_{NI} = T^* + \Delta T^* \quad (6a)$$

$$C_{p,N} = B_C + D_C \left[\frac{T}{T^{**}} - 1 \right] + A_{C,N} \left| \frac{T}{T^{**}} - 1 \right|^{-\alpha} \quad \text{for } T < T_{NI} = T^{**} - \Delta T^{**} \quad (6b)$$

where α is the specific-heat critical exponent, the same at the I and N phases; T^{**} and T^* are spinodal temperatures, being always $T^{**} > T^*$. Both B_C and D_C terms concern to the so-called specific heat background, being identical at both sides of the transition; the last term in both equations is the critical power law divergence and $A_{C,N}$ and $A_{C,I}$ are the corresponding amplitudes. Both ΔT^* and ΔT^{**} , or even better, the difference $(T^{**} - T^*)$ represent the width of the metastable region at the N-to-I phase transition. Common parameters in both phases (B_C, D_C and α) have been simultaneously refined after a previous independent fitting. The most significant parameters ($A_{C,N}/A_{C,I}$; $(T^{**} - T^*)$ and α) that characterize the nature of the N-to-I phase transition are collected in Table 2. All the fitted parameters represent well enough the measured specific-heat data, as indicated by χ^2 values and as is seen in Figure 9 where both eq 6a and 6b are drawn.

The latent heat associated with the N-to-I phase transition is calculated using eq 1 over the specific heat data of Figure 9 through a previous careful calibration.³⁸ The fitted parameters B_C and D_C of $2.13 \text{ J} \cdot \text{g}^{-1} \cdot \text{K}^{-1}$ and $-2.99 \text{ J} \cdot \text{g}^{-1} \cdot \text{K}^{-1}$, respectively, were used to calculate the specific-heat background on eq 1. Our value along with that read from literature is consigned in Table 1. As it can be clearly observed, our calculated latent heat is about

Table 2. Results of the Fittings for the N-to-I Phase Transition

physical magnitude	A_N/A_I	$T^{**} - T^*$ K	α	β	$\chi^2 \times 10^4$
specific heat	2.7 ± 0.1	0.21^a	0.51 ± 0.05	---	2
static permittivity	-0.90 ± 0.02	0.42^a	0.5 ± 0.1	---	0.4
dielectric anisotropy	---	---	---	0.25 ± 0.03	1

^a The error in both magnitudes is estimated to be of about 50% of the absolute magnitude of $(T^{**} - T^*)$.

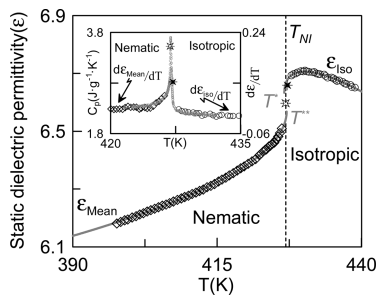


Figure 10. Behavior of the mean static dielectric permittivity in the nematic phase (open diamonds) and the static dielectric permittivity in the isotropic phase (open circles) for CBO11O·Py. Gray solid lines are fittings according to eqs 7a and 7b. The inset shows the derivative of the static dielectric permittivity with temperature (left y-axis and open circles) and specific heat data (right y-axis and gray circles) both as a function of temperature.

three and a half times lower than the value of Attard et al. We should note that the latent heat measured by Attard et al. was made by means of a DSC at $10\text{ K}\cdot\text{min}^{-1}$.

3.3.3. Static Dielectric Permittivity Measurements Analysis. Details of the evolution of the dielectric permittivity data ($\varepsilon_{\text{Mean}}$ and ε_{iso}), already shown in Figure 4, around the N-to-I phase transition are shown in Figure 10. On the I side, ε_{iso} exhibits a maximum which is usually found in liquid crystal monomers with a nearly longitudinal dipole moment.^{38,47}

The data analysis at the N-to-I phase transition has been carried out in a similar way as liquid crystal monomers, according to the following equations^{38,46,47}

$$\varepsilon_{\text{iso}} = \varepsilon^* + a_I |T - T^*| + A_{\varepsilon,I} |T - T^*|^{1-\alpha} \quad \text{for } T > T_{NI} = T^* + \Delta T^* \quad (7a)$$

$$\varepsilon_{\text{mean}} = \varepsilon^{**} + a_N |T - T^{**}| + A_{\varepsilon,N} |T - T^{**}|^{1-\alpha} \quad \text{for } T < T_{NI} = T^{**} - \Delta T^{**} \quad (7b)$$

where α is the specific heat critical exponent, T^* , T^{**} , ΔT^* , and ΔT^{**} have the same meaning as in eq 6 and ε^* and ε^{**} are, respectively, the extrapolated values of ε_{iso} and $\varepsilon_{\text{mean}}$ at T^* and T^{**} , respectively. Both a_I and a_N are the static dielectric permittivity background terms and $A_{\varepsilon,I}$ and $A_{\varepsilon,N}$ are the corresponding dielectric amplitudes. All these parameters can be obtained by fitting the dielectric data and the most significant values ($A_{\varepsilon,N}/A_{\varepsilon,I}$; $(T^{**} - T^*)$ and α) are consigned in Table 2. In our strategy of fitting, the star symbols in Figure 10 have been removed from the fitting according to the scaling relationship between the derivative of the static dielectric permittivity ($d\varepsilon_{\text{mean}}/dT$ and $d\varepsilon_{\text{iso}}/dT$) and the specific-heat (see inset of Figure 10) because they are inside the coexistence region. Such a scaling was theorized by Mistura⁴⁸ and evidenced experimentally in liquid crystal monomers.^{38,46,47} It may be underlined that both

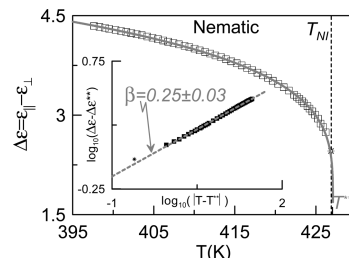


Figure 11. Dielectric anisotropy as a function of temperature. The inset shows a double logarithmic plot of $(\Delta\varepsilon - \Delta\varepsilon^{**})$ vs $(T^{**} - T)$. Gray solid and dashed lines are fittings according to eq 8.

$d\varepsilon_{\text{mean}}/dT$ and $d\varepsilon_{\text{iso}}/dT$ have been obtained numerically by distortion-sensitive derivative analysis.⁴⁷

Both eqs 7a and 7b with the corresponding fitting parameters portray almost perfectly our experimental data as shown in Figure 10.

Figure 11 shows the dielectric anisotropy data ($\Delta\varepsilon$) as a function of temperature in the N mesophase. In liquid crystal monomers, the dielectric anisotropy is usually taken as proportional to the scalar order parameter Q_N ($Q_N = \frac{1}{2}\langle(3\cos^2\theta - 1)\rangle$). The case of CBO11O·Py dimer seems, a priori, more complex. However, it has been observed that in the N-mesophase, the trans conformers population is significantly much higher than the cis conformers and changes very little with temperature. The resulting picture is that the N-mesophase of the dimer seems to be formed by pseudoelongated molecules (trans conformers) with only one dipole moment as in the case of monomers. We should also note how well the static dielectric permittivity behavior with temperature looks like that of a typical monomer with a nearly longitudinal dipole moment. As a consequence, it should be reasonable to consider the dielectric anisotropy of the CBO11O·Py as proportional to the scalar order parameter as well.

The critical behavior of $\Delta\varepsilon$ (or Q_N) at the N-to-I phase transition is usually parametrized, according to the Landau-de Gennes theory^{34,47} as a generic expression

$$\Delta\varepsilon = \Delta\varepsilon^{**} + B |T - T^{**}|^\beta \quad \text{for } T < T^{**} - \Delta T^{**} \quad (8)$$

where T^{**} has the same meaning as in eqs 6b and 7b, and β is the critical exponent. Fittings according to eq 8 of the data consigned in Figure 11 allows us to obtain $\Delta\varepsilon^{**}$, T^{**} , and β (see Table 2). The inset in Figure 11 shows the data of $\log_{10}(\Delta\varepsilon - \Delta\varepsilon^{**})$ as a function of $\log_{10}(T - T^{**})$ as a straight line, the slope of which is the critical exponent β .

3.3.4. Discussion. Biaxial nematic mesophases have been claimed for flexible molecules forming liquid crystals and even their existence has been recently suggested for the dimer α,ω -bis(4-cyanobiphenyl-4'-yl)-heptane.⁴⁹ From our analysis using high-resolution measurements, it has been clearly stated that the nematic mesophase of CBO11O·Py dimer is doubtless

uniaxial because the N-to-I phase transition is of first order in nature. The width of the metastable region ($T^{**} - T^*$), that is linked with the cubic invariant B , has been found to be no null and positive (see Table 2). The value of ($T^{**} - T^*$) from static dielectric permittivity is twice that found from specific heat, as usually occurs. Probably, this is consequence of a nonperfect experimental scaling between the specific heat and the derivative of the static dielectric permittivity, as shown in the inset of Figure 10. Even so, the value of ($T^{**} - T^*$) is of the same order of those reported for the nOCB (alkoxycyanobiphenyls) liquid crystal monomers.⁴⁶ The latent heat (ΔH_{NI}) (see Table 1) is estimated to be similar to the nOCBs as well, despite that the dimers have a conformational contribution to the transition entropy change. Additionally, the transition temperature (T_{NI}) is observed to be nearly 5 K below the value reported by Attard et al.³⁵ At this point, we should note that the entropy change at the N-to-I phase transition is considerably smaller ($\Delta S_{NI}/R = 0.14$) than in other dimeric liquid crystals with conventional rod-like semirigid units and the same spacer.⁵⁰ The most likely explanation is addressed to the high molecular biaxiality induced by the pyrenimine benzylidene unit in the CBO11O·Py dimer. Even so, we wonder how these values would match with those raised from the first theoretical predictions using the rotational isomeric state (RIS) approximation^{19,22} and from most refined approaches.

Regarding the critical behavior of the N-to-I phase transition, the specific heat critical exponent is found to be 0.5 whatever the technique used (either specific heat or static dielectric data). The β -critical exponent of the order parameter through the dielectric anisotropy is found to be 0.25. Both critical exponents are compatible with the tricritical hypothesis. The specific heat amplitude ratio ($A_{C,N}/A_{C,I}$) and even the dielectric amplitude ratio ($A_{\epsilon,N}/A_{\epsilon,I}$) (see Table 2) are in quite agreement with the values obtained for the tricritical behavior in other liquid crystal monomers.^{38,46,51,52}

4. CONCLUSIONS

The study reported in this paper is an extensive investigation of dielectric properties as well as of the N-to-I phase transition of the nonsymmetric dimer (CBO11O·Py) with high molecular biaxiality induced by the pyrenimine benzylidene unit. So far, our dielectric and specific heat measurements are the first performed in compounds of the CBOnO.Py (n being the carbon atoms on the flexible spacer) series.

On the N-mesophase, dielectric results have shown that the permittivity anisotropy is positive. The behavior with temperature of the static dielectric permittivity is observed to be similar to that exhibited by liquid crystal monomers. Dielectric relaxation results have been obtained over a wide range of frequencies from 10^3 to 10^9 Hz. The model of Stocchero et al.¹¹ has allowed to identify and interpret the molecular processes that are responsible for the two different longitudinal dielectric relaxations observed at low frequencies. One of these relaxations, at lower frequencies, is consequence of the flip-flop motion of the larger terminal group of the dimer, while the other relaxation involves a flip-flop of the smaller group. On the basis of the model, a mixture of trans and cis conformers has been evidenced and their relative populations has been calculated as a function of temperature. At higher frequencies, a single mode has been observed in both alignments which has been interpreted as due to precessional motions of the semirigid units of the dimer.

The N-to-I phase transition has been characterized as first-order in nature from specific heat as well as static dielectric permittivity measurements. Despite the biaxiality and flexibility of the molecules, the CBO11O·Py forms a uniaxial nematic mesophase which can be supercooled 36 K down to the I-to-N phase transition. If the cooling rate is of about $15 \text{ K}\cdot\text{min}^{-1}$ or higher, a nematic glassy state is obtained. The measured latent heat associated with the N-to-I phase transition is found to be much lower than the value previously reported in the literature³⁵ and is in agreement with the very weakly first order character of the transition evidenced by the small value of the width of the metastable region.

The evolution with temperature of the orientational order parameter of the uniaxial nematics has been inferred from the data of the dielectric anisotropy. The associated critical exponent is found to be 0.25, the tricritical value. Other strong evidence arising from the specific heat critical exponent and the amplitude ratios ($A_{C,N}/A_{C,I}$) and ($A_{\epsilon,N}/A_{\epsilon,I}$) suggest that the N-to-I phase transition exhibits a tricritical behavior.

■ AUTHOR INFORMATION

Corresponding Author

*E-mail: david.orencio.lopez@upc.edu.

■ ACKNOWLEDGMENT

The authors are grateful for financial support from the MICINN project MAT2009-14636-C03-01,02,03 and from the Gobierno Vasco (GI/IT-449-10). The authors also thank the recognition from the Generalitat de Catalunya of GRPFM as Emergent Research Group (2009-SGR-1243). One of us, N. Sebastián would like to thank the Universidad del País Vasco for a predoctoral grant. We are grateful to Dr. U. Martínez-Estibalez, Universidad del País Vasco, for his assistance in the synthesis of the material.

■ REFERENCES

- (1) Imrie, C. T.; Henderson, P. A. *Curr. Opin. Colloid Interface Sci.* **2002**, *7*, 298–311.
- (2) Imrie, C. T.; Henderson, P. A. *Chem.Soc.Rev.* **2007**, *36*, 2096–2124.
- (3) Imrie, C. T.; Luckhurst, G. R.; *Liquid Crystal Dimers and Oligomers*, in the *Handbook of Liquid Crystals Vol. 2B: Low Molecular Weight Liquid Crystals*, Demus, D., Goodby, J. W., Gray, G. W., Spiess, H. W., Vill, V., Eds.; Wiley-VCH: Weinheim, Germany, 1998; Chapter X, p 801.
- (4) Yelamaggad, C. V.; Prasad, S. K.; Nair, G. G.; Shashikala, I. S.; Rao, D. S. S.; Lobo, C. V.; Chandrasekhar, S. *Angew. Chem., Int. Ed.* **2004**, *43*, 3429–3432.
- (5) Lagerwall, J. P. F.; Giesselmann, F.; Wand, M. D.; Walba, D. M. *Chem. Mater.* **2004**, *16*, 3606–3615.
- (6) Tamba, M. G.; Kosata, B.; Pelz, K.; Diele, S.; Pelzl, G.; Vakhovskaya, Z.; Kresse, H.; Weissflog, W. *Soft Matter* **2006**, *2*, 60–65.
- (7) Umadevi, S.; Sadashiva, B. K.; Murthy, H. N. S.; Raghunathan, V. A. *Soft Matter* **2006**, *2*, 210–214.
- (8) Umadevi, S.; Sadashiva, B. K. *Liq. Cryst.* **2007**, *34*, 673–681.
- (9) Srivastava, R. M.; Neves, R. A. W.; Schneider, R.; Vieira, A. A.; Gallardo, H. *Liq. Cryst.* **2008**, *35*, 737–742.
- (10) Dunmur, D. A.; Luckhurst, G. R.; de la Fuente, M. R.; Diez, S.; Pérez-Jubindo, M. A. *J. Chem. Phys.* **2001**, *115*, 8681–8691.
- (11) Stocchero, M.; Ferrarini, A.; Moro, G. J.; Dunmur, D. A.; Luckhurst, G. R. *J. Chem. Phys.* **2004**, *121*, 8079–8097.
- (12) Coles, H. J.; Pivnenko, M. N. *Nature* **2005**, *436*, 997–1000.

- (13) Takanishi, Y.; Toshimitsu, M.; Nakata, M.; Takada, N.; Izumi, T.; Ishikawa, K.; Takezoe, H. *Phys. Rev. E* **2006**, *74*, 051703.
- (14) Sepelj, M.; Lesac, A.; Baumeister, U.; Diele, S.; Nguyen, H. L.; Bruce, D. W. *J. Mater. Chem.* **2007**, *17*, 1154–1165.
- (15) Ferrarini, A.; Greco, C.; Luckhurst, G. R. *J. Mater. Chem.* **2007**, *17*, 1039–1042.
- (16) Aziz, N.; Kelly, S. M.; Duffy, W.; Goulding, M. *Liq. Cryst.* **2008**, *35*, 1279–1292.
- (17) de la Fuente, M. R.; López, D. O.; Pérez-Jubindo, M. A.; Dunmur, D. A.; Diez-Berart, S.; Salud, J. *J. Phys. Chem. B* **2010**, *114*, 7864–7873.
- (18) Emsley, J. W.; Luckhurst, G. R.; Shilstone, G. N. *Mol. Phys.* **1984**, *53*, 1023–1028.
- (19) Ferrarini, A.; Luckhurs, G. R.; Nordio, P. L.; Roskilly, S. J. *J. Chem. Phys.* **1994**, *100*, 1460–1469.
- (20) Luckhurst, G. R. *Mol. Phys.* **1994**, *82*, 1063–1073.
- (21) Luckhurst, G. R.; Romano, S. *J. Chem. Phys.* **1997**, *107*, 2557–2572.
- (22) Ferrarini, A.; Luckhurst, G. R.; Nordio, P. L.; Roskilly, S. J. *Chem. Phys. Lett.* **1993**, *214*, 409–417.
- (23) Furuya, H.; Okamoto, S.; Abe, A.; Petekidis, G.; Fytas, G. *J. Phys. Chem.* **1995**, *99*, 6483–6486.
- (24) Hohmuth, A.; Schiewe, B.; Heinemann, S.; Kresse, H. *Liq. Cryst.* **1997**, *22*, 211–215.
- (25) Bauman, D.; Wolarz, E.; Bialecka-Florjanczyk, E. *Liq. Cryst.* **1999**, *26*, 45–49.
- (26) Pandey, A. S.; Dhar, R.; Pandey, M. B.; Achalkumar, A. S.; Yelamaggad, C. V. *Liq. Cryst.* **2009**, *36*, 13–19.
- (27) Dunmur, D. A.; de la Fuente, M. R.; Pérez-Jubindo, M. A.; Diez, S. *Liq. Cryst.* **2010**, *37*, 723–736.
- (28) Luckhurst, G. R. *Nature* **2004**, *430*, 413–414.
- (29) Luckhurst, G. R. *Angew. Chem., Int. Ed.* **2005**, *44*, 2834–2836.
- (30) Luckhurst, G. R. *Liq. Cryst.* **2009**, *36*, 1295–1308.
- (31) Freiser, M. J. *Phys. Rev. Lett.* **1970**, *24*, 1041–1043.
- (32) Boccaro, N.; Mejdani, R.; de Seze, L. *J. Phys. (Paris)* **1977**, *38*, 149–151.
- (33) de Gennes, P. G. *The Physics of Liquid Crystals*; Oxford Science Publications: Oxford, U.K., 1994.
- (34) Anisimov, M. A.; *Critical Phenomena in Liquids and Liquid Crystals*; Gordon and Breach Science Publishers: Amsterdam, 1991, and references therein.
- (35) Attard, G. S.; Imrie, C. T. *Chem. Mater.* **1992**, *4*, 1246–1253.
- (36) Sied, M. B.; Salud, J.; López, D. O.; Barrio, M.; Tamarit, J. Ll. *Phys. Chem. Chem. Phys.* **2002**, *4*, 2587–2593.
- (37) Puertas, R.; Rute, M. A.; Salud, J.; López, D. O.; Diez, S.; Van Miltenburg, J. C.; Pardo, L. C.; Tamarit, J. Ll.; Barrio, M.; Pérez-Jubindo, M. A.; et al. *Phys. Rev. B* **2004**, *69*, 224202.
- (38) Cusmin, P.; de la Fuente, M. R.; Salud, J.; Pérez-Jubindo, M. A.; Diez-Berart, S.; López, D. O. *J. Phys. Chem. B* **2007**, *111*, 8974–8984.
- (39) Maier, W.; Meier, G. Z. *Naturforsch A* **1961**, *16*, 262–267.
- (40) Nordio, P. L.; Rigatti, G.; Segre, U. *Mol. Phys.* **1973**, *25*, 129–136.
- (41) Diez, S.; Pérez-Jubindo, M. A.; de la Fuente, M. R.; López, D. O.; Salud, J.; Tamarit, J. Ll. *Chem. Phys. Lett.* **2006**, *423*, 463–469.
- (42) Diez, S.; Pérez-Jubindo, M. A.; de la Fuente, M. R.; López, D. O.; Salud, J.; Tamarit, J. Ll. *Liq. Cryst.* **2006**, *33*, 1083–1091.
- (43) Maier, W.; Saupe, A. Z. *Naturforsch. A* **1958**, *13*, 564–566.
- (44) Merkel, K.; Kocot, A.; Vij, J. K.; Mehl, G. H.; Meyer, T. *Phys. Rev. E* **2006**, *73*, 051702.
- (45) Keyes, P. H.; Shane, J. R. *Phys. Rev. Lett.* **1979**, *42*, 722–725.
- (46) Salud, J.; Cusmin, P.; de la Fuente, M. R.; Pérez-Jubindo, M. A.; López, D. O.; Diez-Berart, S. *J. Phys. Chem. B* **2009**, *113*, 15967–15974.
- (47) Rzoska, S. J.; Ziolo, J.; Sulkowski, W.; Jadzyn, J.; Czechowski, G. *Phys. Rev. E* **2001**, *64*, 052701.
- (48) Mistura, L. *J. Chem. Phys.* **1973**, *59*, 4563–4564.
- (49) Cestari, M.; Diez, S.; Dunmur, D. A.; Ferrarini, A.; de la Fuente, M. R.; Jackson, D. A.; Lopez, D. O.; Luckhurst, G. R.; Perez-Jubindo, M. A.; Richardson, R. M.; et al. *23rd International Liquid Crystal Conference*; Krakow, Poland, July 2010, oral communication, p 448.
- (50) Imrie, C. T. *Liquid Crystal Dimers; In the Handbook of Structure and Bonding*; Springer Verlag: Berlin and Heidelberg, Germany; 1999, Vol. 95.
- (51) Diez, S.; López, D. O.; de la Fuente, M. R.; Pérez-Jubindo, M. A.; Salud, J.; Tamarit, J. Ll. *J. Phys. Chem. B* **2005**, *109*, 23209–23217.
- (52) Iannacchione, G. S.; Finotello, D. *Phys. Rev. E* **1994**, *50*, 4780–4795.